Polymer Testing 61 (2017) 258–268

Contents lists available at ScienceDirect

Polymer Testing

journal homepage: www.elsevier.com/locate/polytest

Material Behaviour

A study of rubber flow in a mold during the tire shaping process using experiment and computer simulation

Sung Hyun Choi [a], Min-Young Lyu [b,*]

[a] Hankook Tire Co., LTD., 50 Yuseong-daero 935 beon-gil, Yuseong-gu, Daejeon 34127, South Korea
[b] Department of Mechanical System Design Engineering, Seoul National University of Science and Technology, 232 Gongneung-ro, Nowon-gu, Seoul 01811, South Korea

ARTICLE INFO

Article history:
Received 18 April 2017
Accepted 23 May 2017
Available online 25 May 2017

Keywords:
Tire tread
Tread rubber
White rubber strip
Shaping process
Green tire
Computer simulation

ABSTRACT

Automobile tires consist of more than ten layers, including tread, belt, carcass, sidewall, etc. The outermost layer, known as the tread, plays an important role during driving as it comes in direct contact with the road. This tread has grooves with complicated shapes, which are formed by a mold during the shaping process. When the tread rubber does not fill the mold properly, tire quality deteriorates crucially. As such, it is important to observe the flow of the tread rubber during the shaping process. To determine the flow of tread rubber in the mold, we conducted an experiment and computer simulation with white rubber strips inserted into specific areas of the tread. The white rubber strips showed detailed flow behavior of the tread rubber visually in the mold during the shaping process. No significant flows were observed for rubber in the central area of each block of the mold, but more changes were found near the edges of each block. The strips of rubber below the grooves exhibited more significant changes as they were pressed down by the protruding area of the mold. Moreover, there was no flow of rubber between blocks in the mold. This implies the profile design of the extruded tread should match the mold profile and the volume of each block. The experiment and simulation had similar results, and the observations of rubber flow in the mold using simulation proved to be highly useful.

1. Introduction

Tires are a key component of automobiles. They come in direct contact with the road and have a significant influence on vehicle performance, including braking force, handling and noise [1–5]. Automobile tires are designed to handle various road conditions, and are available as all-season tires, snow tires, mountain tires and mud tires. The shaping of these tires surfaces is very complex, and inadequate rubber flow during tire manufacturing can result in defective tires [6–8].

The manufacturing of automobile tires begins with the mixing process, which combines crude rubber with carbon black, sulfur, etc. to form a rubber with desirable properties. This is followed by the extrusion process, which produces layers that have the characteristics of each tire component. The rubber layers are then wound to form a cylindrical green tire (GT). Lastly, the GT undergoes vulcanization to become a tire with a designed balance of elasticity and rigidity through the curing process. During the curing process, an expansion tube (bladder) is fitted inside the GT. When high-pressure steam is applied to the bladder, the GT expands onto the mold, adopting its shape, and forming a tire with a complex and unique groove on the tread layer [9,10]. Since the final shape of the tire is determined during the curing process, it is also known as the shaping process.

A typical automobile tire consists of more than ten layers (tread rubber, carcass rubber, inner liner rubber, sidewall rubber, rim cushion rubber, bead rubber, bead filler rubber, etc.). The outermost tread layer, which comes into direct contact with the road, consists of a main groove, sub groove and kerf. Poor fitting of the rubber into the mold during the shaping process can result in defects, which affect tire performance. In turn, this causes problems with overall vehicle performance, such as braking force, handling and noise [11–15]. Assessing rubber flow is thus very important to ensure the proper treading of tires during the shaping process.

* Corresponding author.
E-mail address: mylyu@seoultech.ac.kr (M.-Y. Lyu).

http://dx.doi.org/10.1016/j.polymertesting.2017.05.030

There have been numerous studies on tire design, performance and production. J. K. Lee and D. M. Kim analyzed friction on tire tread and stress on tires during driving [2,16–19]. K.W. Kim and B. S. Kim studied standing waves in relation to tread patterns and the relationship between groove arrangement and noise [15,20–22]. Extrusion, one of the rubber layer shaping processes required for tire manufacturing, has been extensively studied [23–25]. However, little published research exists on the prediction of rubber flow in a mold during the shaping process. Recently, a computer simulation of rubber flow during the shaping process has been suggested and performed [26]. This research was a very limited simulation, and no experimental verifications were involved.

The present study is an extension of that previous work, and examines in detail the rubber flow in the outermost tread layer of the GT during the shaping process, both experimentally and theoretically. White rubber strips were locally inserted in the tread rubber layer to allow visualization of the rubber flow. Observations were made on the specific flow of the tread rubber in the mold, and the simulation was compared with experimental

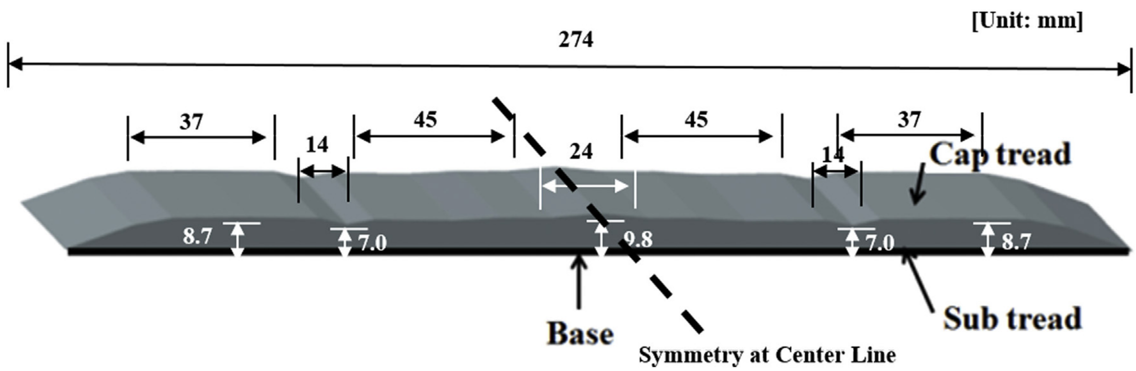

Fig. 1. Tread rubber layer (Cap Tread and Sub Tread) and its base.

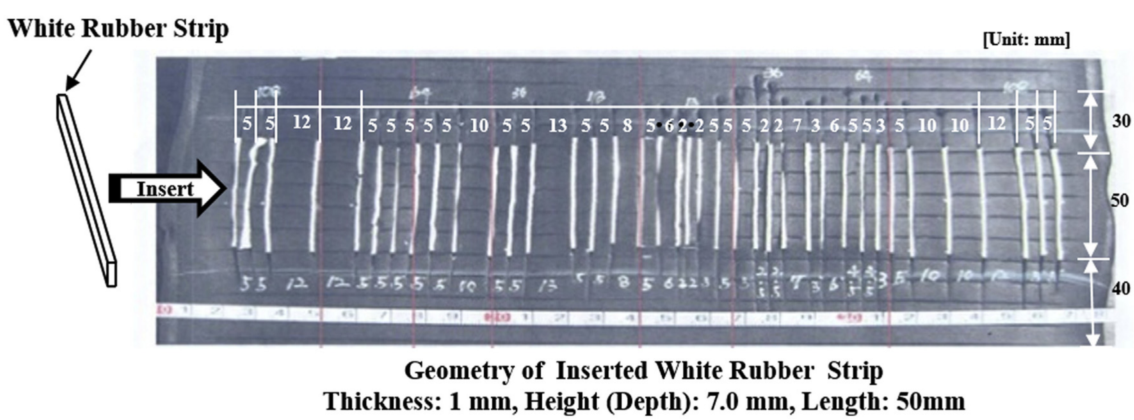

Fig. 2. White rubber strips inserted into the base of the tread rubber layer.

Fig. 3. Cross-sectional shape of the green tire (Model: 255/55R18V RH07).

results. Research results obtained in this study can provide a detailed understanding of rubber flow in a complicated mold, and this also serves as a guide-line for the profile design of the tread layer.

2. Experimental model and computer simulation

2.1. Experimental

2.1.1. Experimental model

An experiment was conducted to observe the flow of tread rubber in the mold during the shaping process. To visualize the flow of rubber, white rubber strips were inserted inside the black tread rubber layer (the tread rubber layer consists of a cap tread and a sub tread) as shown in Fig. 1 and Fig. 2. Changes in the shape of the white rubber strips were analyzed after the shaping process. Fig. 1 shows the geometry and dimensions of the tread rubber layer for tire model 255/55R18V RH07 (Hankook Tire Co.). The white rubber strips were inserted into the base of the tread rubber layer. The number of inserted white rubber strips was thirty-eight, and each of the white rubber strips had a thickness of 1.0 mm and a height of 7.0 mm from the base of the tread rubber layer. Fig. 2 shows the white rubber strips inserted into the base of the tread rubber layer.

The GT used in this experiment was comprised of nine layers: cap tread, sub tread, nylon full cover (NFC), composite, carcass, inner liner, side wall, bead, and bead filler. The cross-sectional shape of the GT is shown in Fig. 3. The tread rubber layer (cap tread and sub tread) containing the white rubber strips shown in Figs. 1 and 2 was the outermost layer of the GT shown in Fig. 3. The detailed geometries of the layers are described in Section 2.2.2 Simulation Model.

The mold for shaping the tire is shown in Fig. 4. To manufacture the tire, the GT shown in Fig. 3 is inserted into the mold shown in Fig. 4 and the GT is inflated using steam. The inflated GT becomes a tire. Fig. 4 shows the geometry of the mold containing six grooves. The mold is divided into seven blocks by the six grooves, with V-grooves at both ends (groove 1 and groove 6) and four U-grooves (groove 2, groove 3, groove 4, and groove 5) in the middle.

Table 1
Viscosity by rubber layer.

Layer	Viscosity [Pa·s]
Cap Tread	53,986
Sub Tread	28,107
NFC	200,000
Composite	10,000,000
Carcass	800,000
Inner Liner	24,447
Bead	1,000,000,000
Bead Filler	47,844
Sidewall	27,407
Bladder	683,630
White rubber	27,407

Table 2
Modified viscosities of NFC layer and composite layer.

Item	Layer	Modified viscosity [Pa·s]
Case 1	NFC	20,000,000
Case 2	NFC	20,000,000
	Composite	1,000,000,000

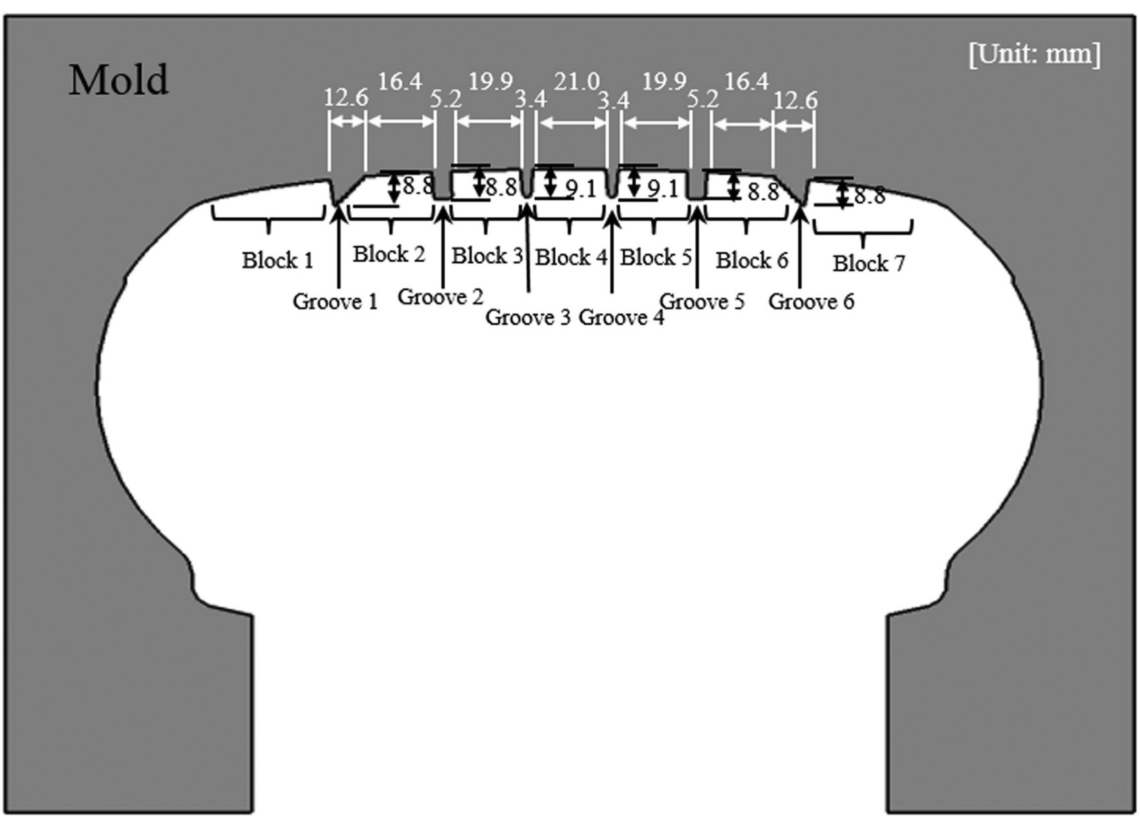

Fig. 4. Profile of the mold containing six grooves and seven blocks.

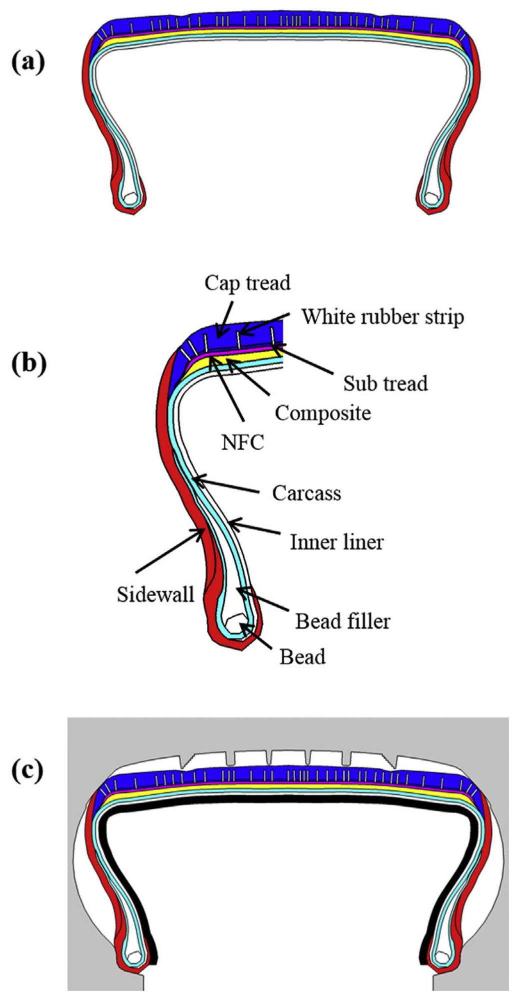

Fig. 5. Simulation model of GT containing white rubber strips and mold with bladder. (a) GT model containing white rubber strips in the tread rubber layer. (b) Detail of GT layers with white rubber strips. (c) Mold, GT, and bladder for shaping the tire.

2.2. Computer simulation

2.2.1. Governing equation and constitutive equation

The flow of the polymer melt follows the equations of motion, and Eq. (1) is the equation of motion in a rectangular coordinate system [27,28]:

$$\frac{\partial(\rho u)}{\partial t} + \nabla\cdot(\rho u \vec{v}) = \left(-\frac{\partial p}{\partial x} + \frac{\partial \tau_{xx}}{\partial x} + \frac{\partial \tau_{yx}}{\partial y} + \frac{\partial \tau_{zx}}{\partial z} \right) + \rho f_x \tag{1a}$$

$$\frac{\partial(\rho v)}{\partial t} + \nabla\cdot(\rho v \vec{v}) = \left(-\frac{\partial p}{\partial y} + \frac{\partial \tau_{xy}}{\partial x} + \frac{\partial \tau_{yy}}{\partial y} + \frac{\partial \tau_{zy}}{\partial z} \right) + \rho f_y \tag{1b}$$

$$\frac{\partial(\rho w)}{\partial t} + \nabla\cdot(\rho w \vec{v}) = \left(-\frac{\partial p}{\partial z} + \frac{\partial \tau_{xz}}{\partial x} + \frac{\partial \tau_{yz}}{\partial y} + \frac{\partial \tau_{zz}}{\partial z} \right) + \rho f_z \tag{1c}$$

where u, v, and w are, respectively, the velocities in the x, y, and z directions, and τ is the extra stress, whose relationship to the total stress σ is shown in Eq. (2):

$$\sigma = -p\underline{I} + \tau \tag{2}$$

where p is the hydrostatic pressure and $\mathbf{I}$ is the unit tensor.

In the tire shaping process, the material flow is slow and the shear rate is considered to be very low. Thus, the rheological model used in this study is the Newtonian model, and the extra stress can be expressed by Eq. (3) [11,12]:

$$\tau = 2\eta D \tag{3}$$

where η is the viscosity and D is the rate of deformation tensor.

Table 1 shows the viscosity of each rubber layer. The rubber is cross-linked during the actual shaping process, but the changes in physical properties during this process were neglected in this study.

The simulation was carried out with varying viscosity for a more detailed examination of the flow of tread rubber. The viscosity of the NFC layer was increased in Case 1, while the viscosity of both the NFC layer and the composite layer was increased in Case 2. Table 2 shows the modified viscosities of the NFC layer and

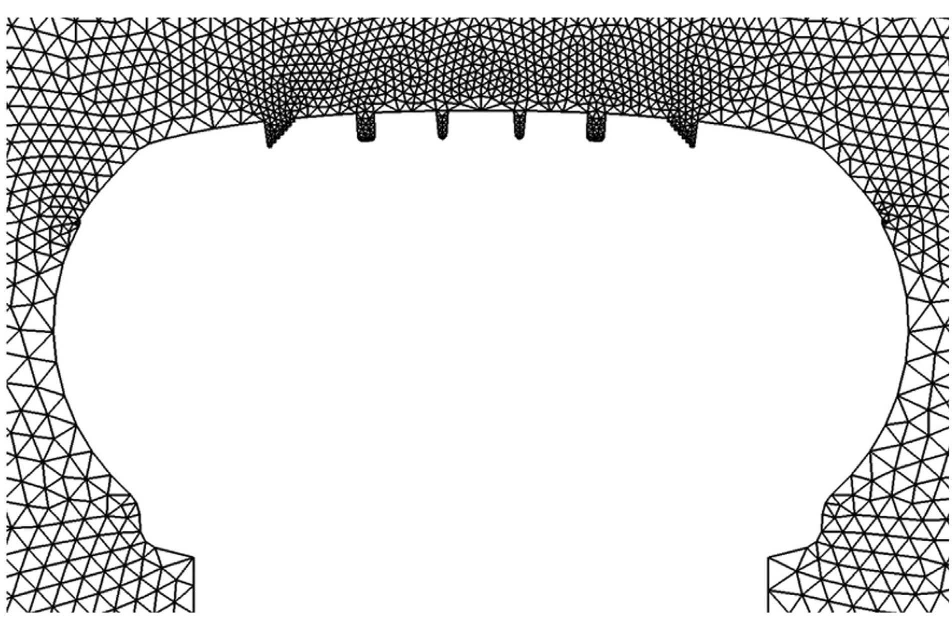

Fig. 6. Mesh shape in mold for computer simulation.

composite layer for further simulation.

2.2.2. Simulation model

To simulate the rubber flow observed in the experiment, a simulation was performed under the same conditions as those in the experiment. The simulation model for the GT containing the white rubber strips, and the mold, is given in Fig. 5. Similar to the experiment, the cap tread coming in contact with the mold had a flat shape. The mold had V-grooves at both ends and four U-grooves in the middle, as shown in Fig. 4. Small grooves (sub groove, kerf) included in the actual mold were excluded. A total of thirty eight pieces of white rubber strips were inserted into the base of the tread rubber layer, as shown in Fig. 2. Fig. 5(a) and (b) present the modeling of the nine rubber layers and white rubber strips. The simulation took into account ten rubber layers, thirty eight white rubber strips and the bladder, as shown in Fig. 5(c), which is subjected to pressure during shaping and enables the GT to fit into the mold.

2.2.3. Mesh generation and boundary conditions

Polyflow, a software for computational fluid dynamics (CFD) supplied by Ansys, was used in the 2D axisymmetric simulation. It was a moving boundary problem and the simulation was performed as a time-dependent problem to analyze rubber flow over time during the shaping process.

The mesh shapes in the mold and the GT are presented in Fig. 6 and Fig. 7, respectively. The simulation involved triangular meshes suited for remeshing. The rubber layers had more densely constructed meshes compared to the mold. To observe the flow of the white rubber strips, meshes were densely distributed for the white rubber strips and their surroundings. Fig. 7 shows meshes for the entire region of the GT and for detailed regions of the GT.

The four boundary conditions applied were contact, moving interface, normal and tangential velocity, and normal force. Fig. 8 shows the initial shape of the GT including the bladder which is the same as the mold and GT including bladder shown in Fig. 5(c), and the location at which each boundary condition was applied. To stick the outermost layer of the GT onto the mold, the contact condition was applied to BC1 (Fig. 8 (a)), and the mold surface was subjected to the no-slip condition. A moving interface was applied to all boundaries between each rubber layer, BC2 in Fig. 8 (b). On both ends of the bladder, BC3 in Fig. 8 (c), the normal velocity and tangential velocity were set to zero. This means BC3 is fixed. BC4 in Fig. 8 (d) is the outer surface of the bladder on which 17kg$_f$/cm^2 of pressure was applied.

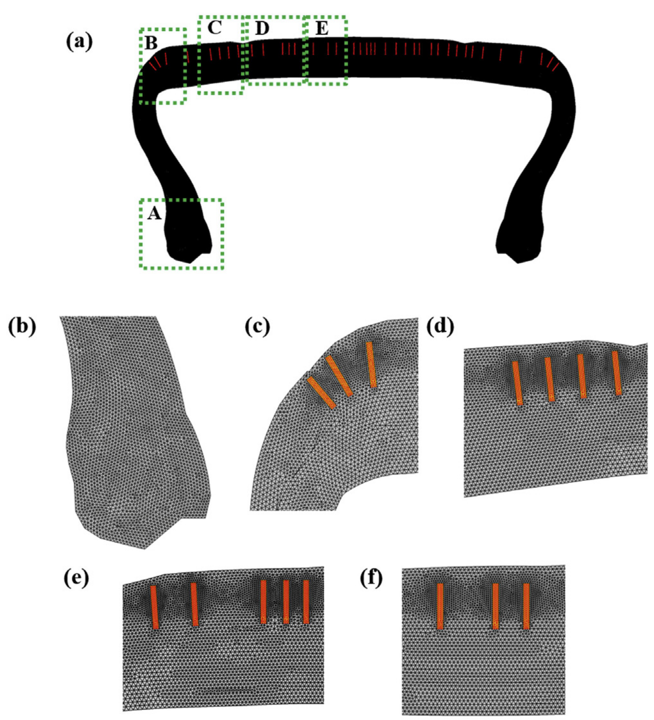

Fig. 7. Mesh shapes for the entire region of the GT and detailed regions of the GT used for computer simulation. (a) Meshes in the entire region of the GT. (b) Detail of meshes in region 'A'. (c) Detail of meshes in region 'B' containing the white rubber strips. (d) Detail of meshes in region 'C' containing the white rubber strips. (e) Detail of meshes in region 'D' containing the white rubber strips. (f) Detail of meshes in region 'E' containing the white rubber strips.

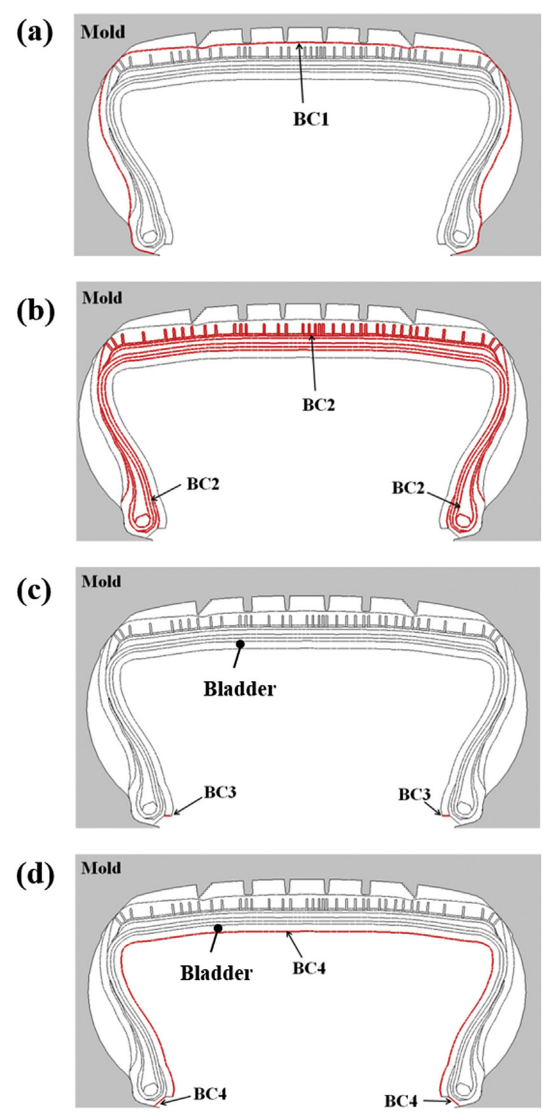

Fig. 8. Locations of the four boundary conditions. (a) Boundary condition 1 (BC1): Contact surface. (b) Boundary condition 2 (BC2): Moving interface. (c) Boundary condition 3 (BC3): Exert a normal and tangential velocity. (d) Boundary condition 4 (BC4): Exert a normal force.

3. Results and discussion

3.1. Experimental results

Fig. 9(a) shows the exterior of the completed tire and Fig. 9(b) shows the cross-section of the completed tire as indicated in Fig. 9(a). Deformations of the white rubber strips can be observed clearly in the cross-section of the completed tire. These observations represent the detailed flow behavior of the tread rubber in the mold. Large deformations in the tread rubber can be observed near the six grooves of the mold, whereas little deformation is observed in the blocks of the mold, as shown in Fig. 9(b). Fig. 10 shows the detailed deformations in the white rubber strips in each block and groove of the mold. The white rubber strips in the block of the mold remain perpendicular to the mold surface, which is the same as their original state. White rubber strips located near the groove in each block were slightly bent in the direction of the block edges. In other words, some changes were observed in the tread rubber near the groove, but there was no relocation into other blocks.

The white rubber strips below the grooves exhibited significant changes. As the tread rubber came into contact with the mold, the tread rubber was squashed by the grooves. Below the grooves, there was no sign of the white rubber moving to other blocks, indicating that rubber does not move between blocks during the shaping process. This implies that the external profile of the tread layer should be designed to match the mold shape and volume of each block in the mold.

3.2. Computational results

3.2.1. Settling of tread rubber in the mold

Fig. 11 shows the computational result when the shaping process was completed. The GT containing white rubber strips was completely in contact with the mold surface and produced patterns on the tire surface. The straight white rubber strips are bent and squashed. Deformations of the white rubber strips are similar to the experimental observation shown in Fig. 9(b).

Observations were made on the settling order of the tread rubber in the blocks of the mold during the shaping process. Fig. 12 shows the computational results of the tread area of the completed tire divided into seven blocks, numbered from ① to ⑦, and as compared with the experimental results. The tread area was divided into blocks along the grooves. The order of settling was compared across the seven blocks. The fastest settling time was observed in block ④ in the mold (settling time: 0.003942 s). The next blocks were blocks ② and ⑥ in the mold (settling time: 0.004173 s), followed by blocks ③ and ⑤ in the mold (settling time: 0.004866 s), and finally, blocks ① and ⑦ in the mold (settling time: 0.005212 s). Since the tire is symmetrical around the center, the settling time was also found to be symmetrical. The computational results and experimental results are in good agreement.

3.2.2. Velocity distribution of the tread rubber

Fig. 13 shows the velocity vector of the tread rubber flow in the block when the shaping process was 95% completed. After the rubber settles in the center region of each block, rubber flow is divided and flows to the edges. In this process, white rubber

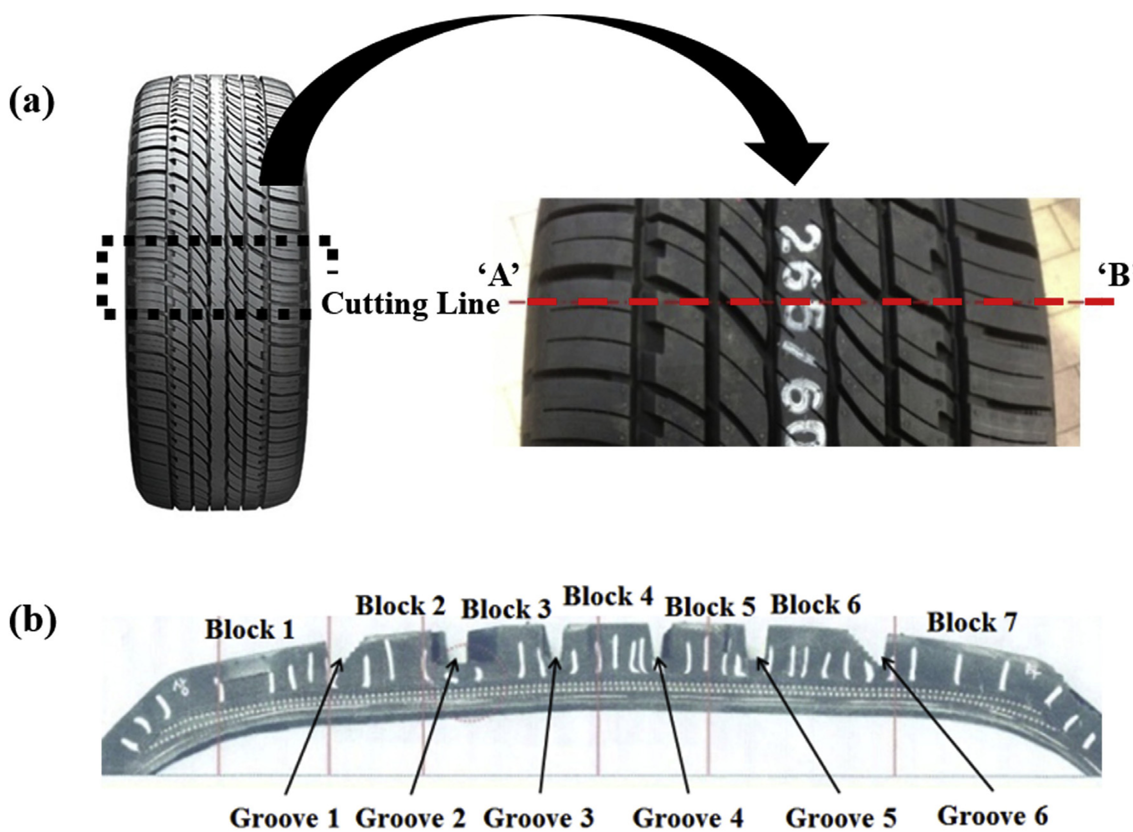

Fig. 9. Shape and cross-section of the completed tire. (a) Shape of completed tire and location of cutting line, A-B. (b) Cross-section of the completed tire.

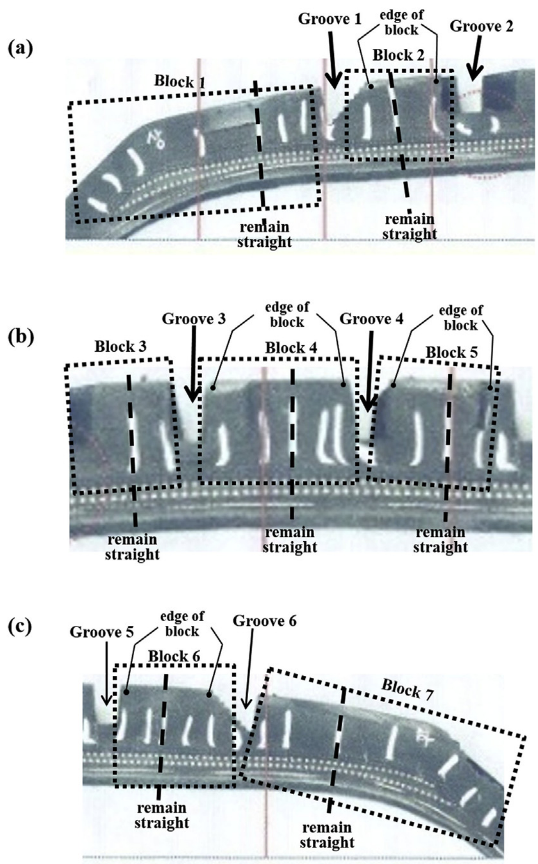

Fig. 10. Deformations of the white rubber strips in each block and groove of the mold. (a) At block 1, block 2, groove 1, and groove 2. (b) At block 3, block 4, block 5, groove 3, and groove 4. (c) At block 6, block 7, groove 5, and groove 6.

strips head towards the direction of the edges of each block. This caused the white rubber strips in the blocks to bend in the direction of the edges during the shaping process, as shown in Fig. 10. The simulation results are consistent with experimental observation.

Fig. 14 shows the velocity vector of rubber flow near the grooves at 95% completion of shaping. Since rubber settles at similar rates in blocks on the left and right of grooves, the white rubber does not sway to one side. The groove presses the white rubber, and rubber flow is not observed between blocks.

The experiment also showed the pressing of the white rubber near the grooves, as shown if Fig. 10, showing that the simulated results coincided with the experiment.

3.2.3. Changes in rubber flow with varying viscosity

Fluid flow is influenced by viscosity. Thus, the flow behavior of the tread rubber layer mainly depends on its viscosity. It is also affected by its neighboring layers. The NFC and composite layers are located just under the tread (cap tread and under tread) layer. Flow simulations of the GT during the shaping process with varying viscosities of NFC and composite layers were conducted to investigate the flow behaviors of the tread rubber in the mold.

Fig. 15 shows the simulation result when the viscosity of just the NFC layer was increased, which corresponds to case 1 in Table 2. When the viscosity of the NFC layer was increased, blocks ② and ⑥ in the mold had the fastest settling time (settling time: 0.004096 s). The next was block ④ in the mold (settling time: 0.004327 s), followed by blocks ① and ⑦ in the mold (settling time: 0.007271 s), and finally, blocks ③ and ⑤ in the mold (settling time: 0.007791 s). No significant change was found in the shapes of the white rubber strips when the results for the unmodified (original) viscosity were compared with the increased NFC viscosity (Fig. 12 vs. Fig. 15). Despite the increased viscosity of the NFC layer, there was minimal influence on the shape of the tread rubber, since the NFC layer takes up only a small volume in the GT.

Fig. 16 shows the simulation result for increased viscosities of both the NFC and composite layers, which is case 2 in Table 2. The settling order in the tread area was changed in relation to changes

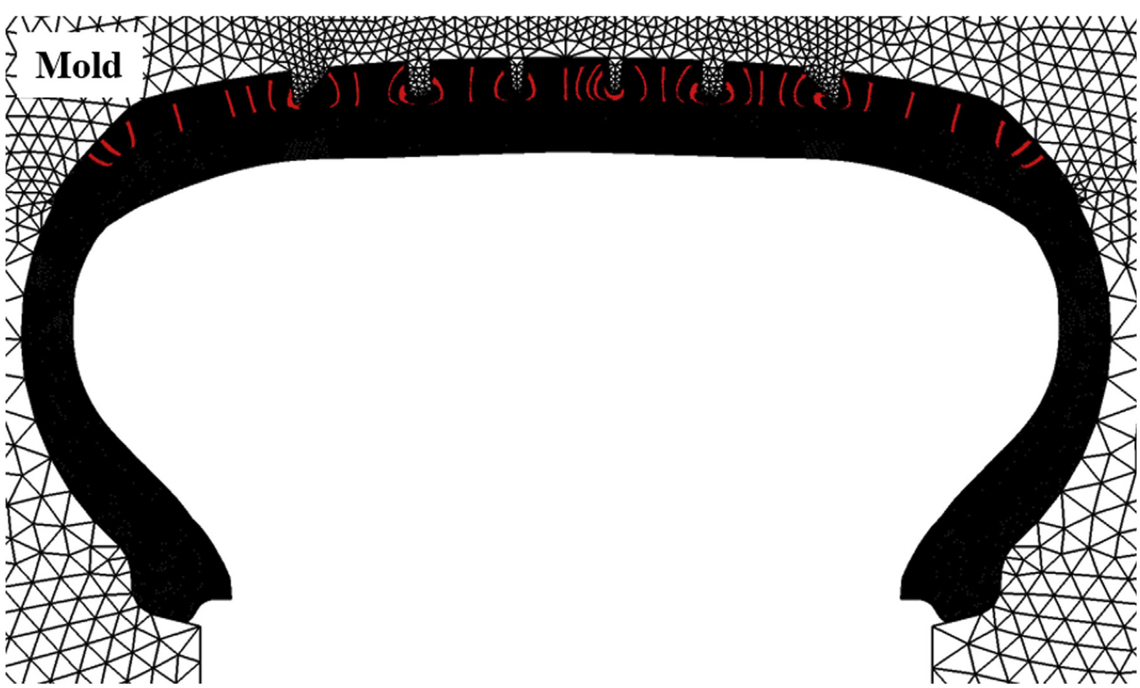

Fig. 11. Results of the simulation of the final stage of the tire shaping process, showing deformation of the white rubber strips in the tread rubber.

in the viscosities of the NFC and composite layers. When the viscosities of both the NFC and composite layers were increased, blocks ① and ⑦ had the fastest settling time (settling time: 0.038140 s). The next blocks were blocks ② and ⑥ (settling time: 0.039701 s), followed by blocks ③ and ⑤ (settling time: 0.042978 s), and finally, the central block ④ (settling time:

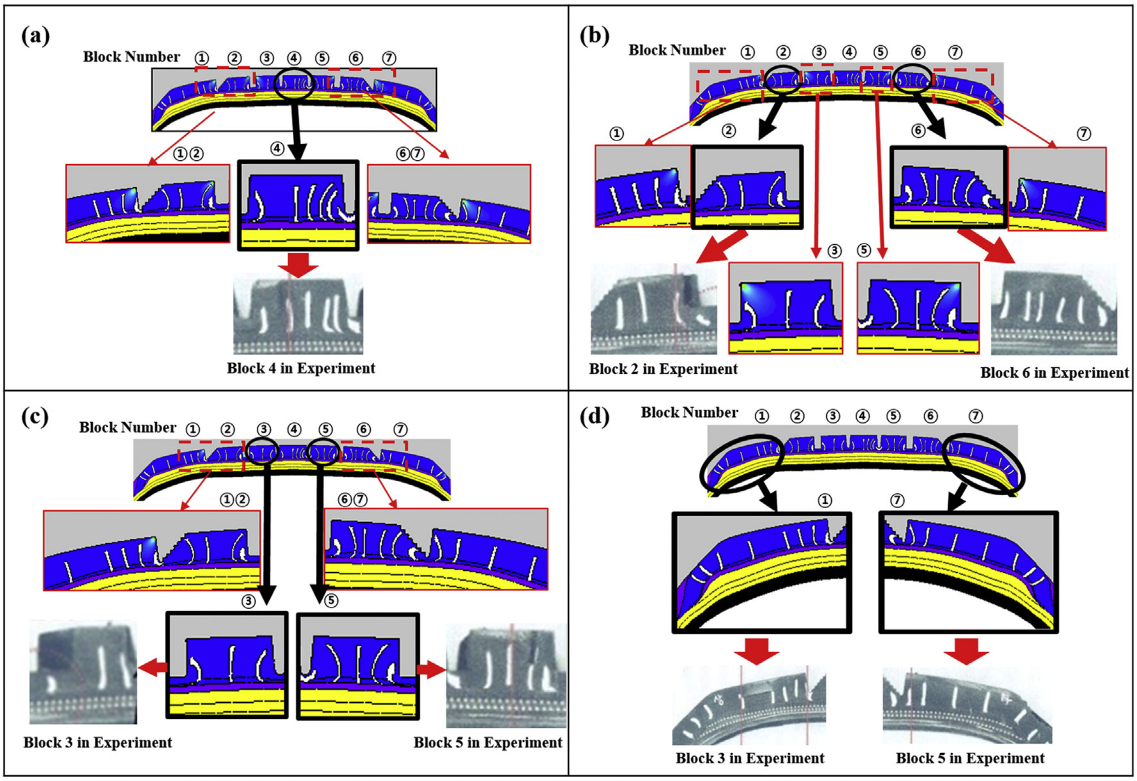

Fig. 12. Computational results of tread rubber settling in the block of the mold and in comparison to the experiment. (a) Settling in block 4. (b) Settling in block 2 and block 6. (c) Settling in block 3 and block 5. (d) Settling in block 1 and block 7.

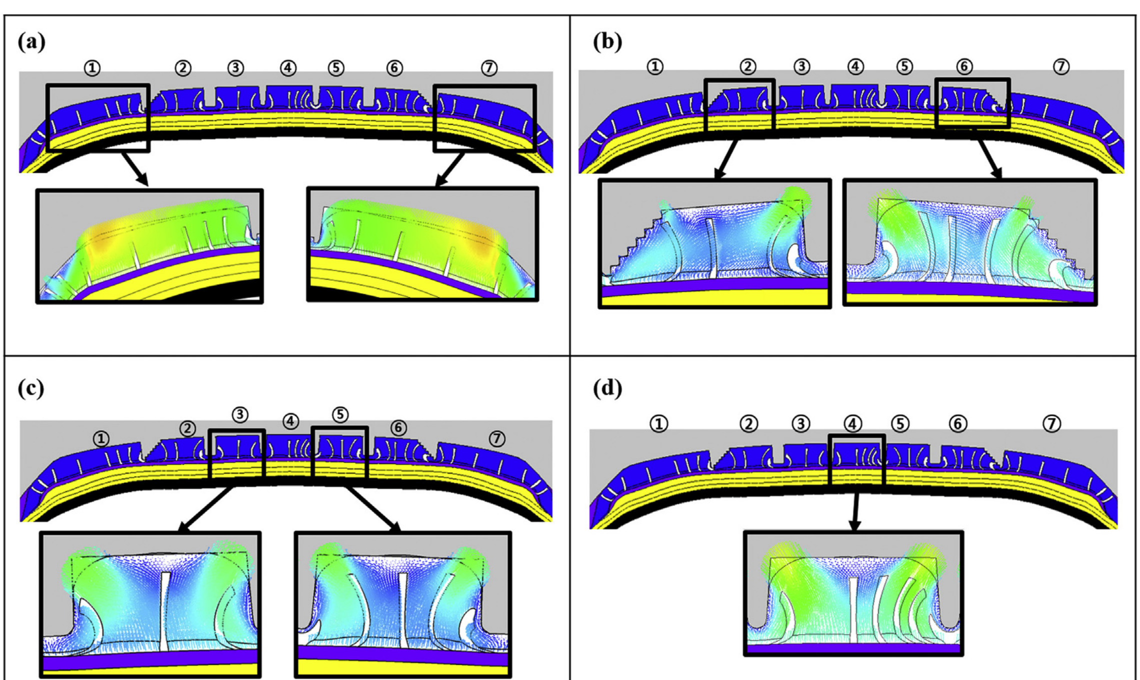

Fig. 13. Velocity vector of rubber flow in blocks at 95% completion of shaping. (a) Settling in block 1 and block 7. (b) Settling in block 2 and block 6. (c) Settling in block 3 and block 5. (d) Settling in block 4.

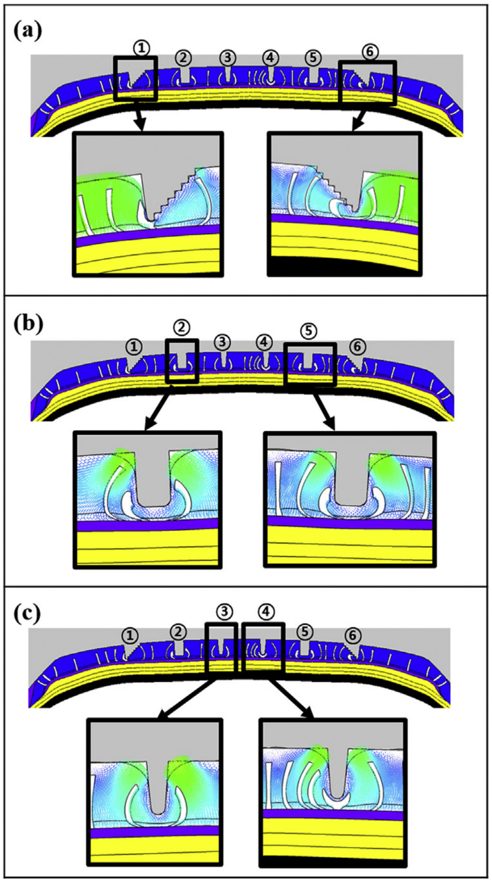

Fig. 14. Velocity vector of rubber flow near the grooves at 95% completion of shaping. (a) Settling in groove 1 and groove 6. (b) Settling in groove 2 and groove 5. (c) Settling in groove 3 and groove 4.

0.061397 s). When the viscosities of both the NFC and composite layers were increased, the shapes of the white rubber strips in blocks ① and ⑦ in the mold bent, whereas the white rubber strips in blocks ① and ⑦ in the mold did not bend with either the original viscosity (shown in Fig. 12) or when the viscosity of the NFC layer was increased (shown in Fig. 15). Among the tire layers, the composite takes up a relatively large volume, and thus has a significant influence on the tread rubber flow.

Fig. 17 shows the settling of rubber in the shoulder and tread areas with unmodified (original) viscosity, increased viscosity of the NFC layer, and increased viscosity of both the NFC and composite layers. When the simulation was performed with the unmodified (original) viscosity and with the increased NFC layer viscosity, the rubber settled in the mold with flow occurring in both the shoulder and tread areas, as shown in Fig. 17(a) and (b). When the viscosity was increased in both the NFC and composite layers, the rubber in the shoulder area first settled in the mold, and then rubber began to flow into the tread area, as shown in Fig. 17 (c). When the viscosity of both the NFC and composite layers was increased, the flow in the tread area became slower, since the NFC and composite layers are located just below the tread layer, whereas there are no NFC and composite layers in the shoulder area. Rubber flow first occurred in the shoulder area followed by the tread area. Due to this flow of rubber, the white rubber strips bent in the central direction as shown in blocks ① and ⑦ of Fig. 16(a). During shaping of the GT, rubber flow was influenced by the viscosity of each layer, and the settling order in the mold also depended on the level of viscosity.

4. Conclusion

This study observed the flow of tread rubber during the shaping process using experiment and simulation. A novel method was adopted to examine the flow of tread rubber visually

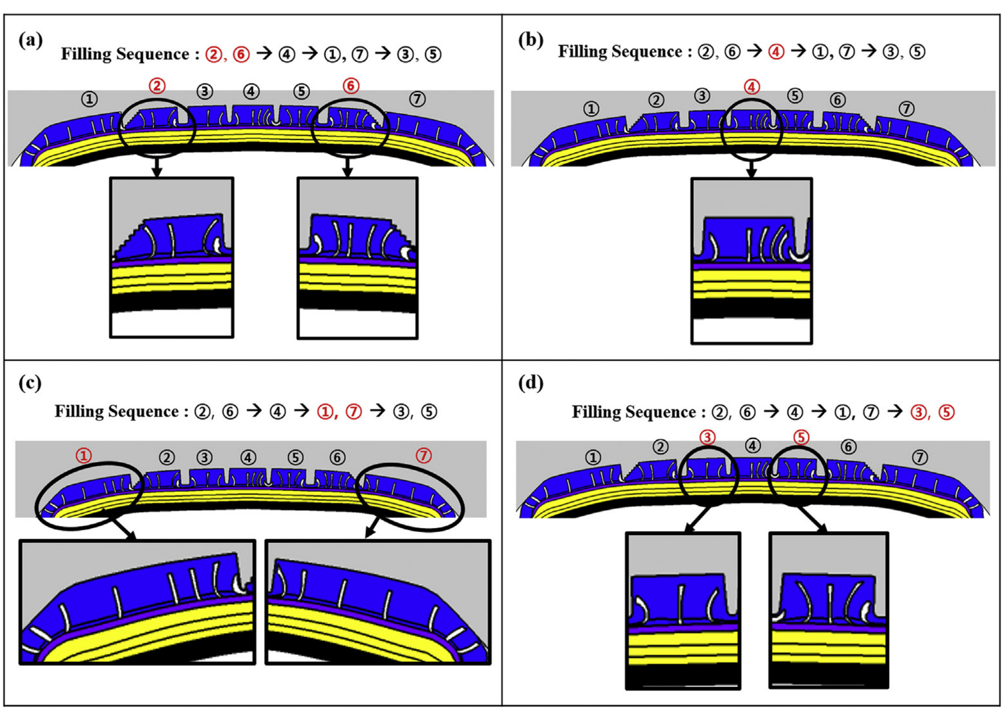

Fig. 15. Flow behavior and mold filling sequence of tread rubber in the block of the mold with increased NFC viscosity. (a) Settling in block 2 and block 6. (b) Settling in block 4. (c) Settling in block 1 and block 7. (d) Settling in block 3 and block 5.

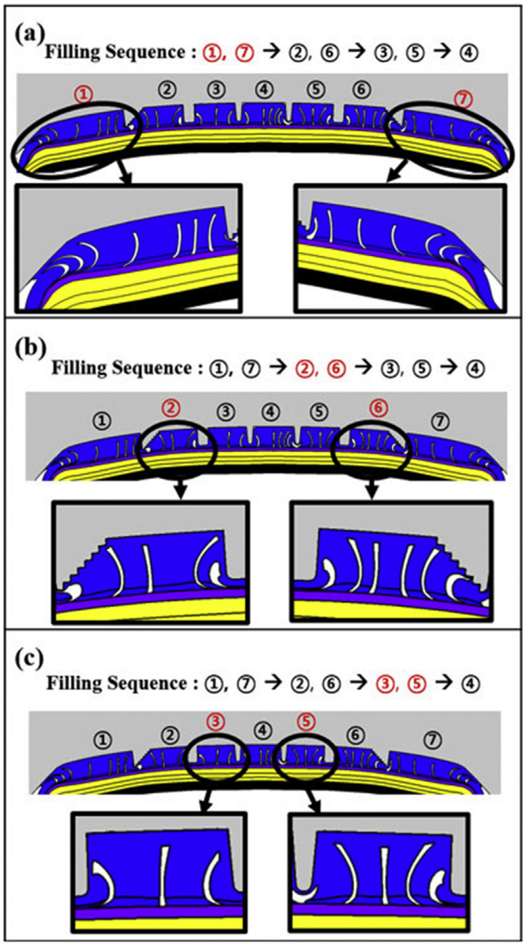

Fig. 16. Flow behavior and mold filling sequence of tread rubber in the blocks of the mold, with increased viscosities of both the NFC and composite layers. (a) Settling in block 1 and block 7. (b) Settling in block 2 and block 6. (c) Settling in block 3 and block 5.

during the shaping process. The flow of rubber during the shaping process was visualized by inserting white rubber strips into the black tread rubber. The shaping process of the GT was observed, and comparisons were made between the experiment and simulation.

In the results, the middle portion of each block of the mold did not show much rubber flow, but flow was observed in the direction of the edges in both the experiment and simulation. At the grooves separating the blocks, the rubber was pressed and significantly deformed. There was no rubber flow between blocks along the grooves. This implies that the profile of the tread layers should be designed to match the geometry of the mold and the volume of each block in the mold.

Because the shape of the GT changes in relation to the viscosities of the rubber layers, it is possible to predict the different settling orders in the mold. The viscosities of the rubber layers in the GT can be seen as having an influence on the final shape and settling orders in the mold.

The method proposed in this study enabled detailed observations of rubber flow, and the results between the experiment and simulation were highly consistent.

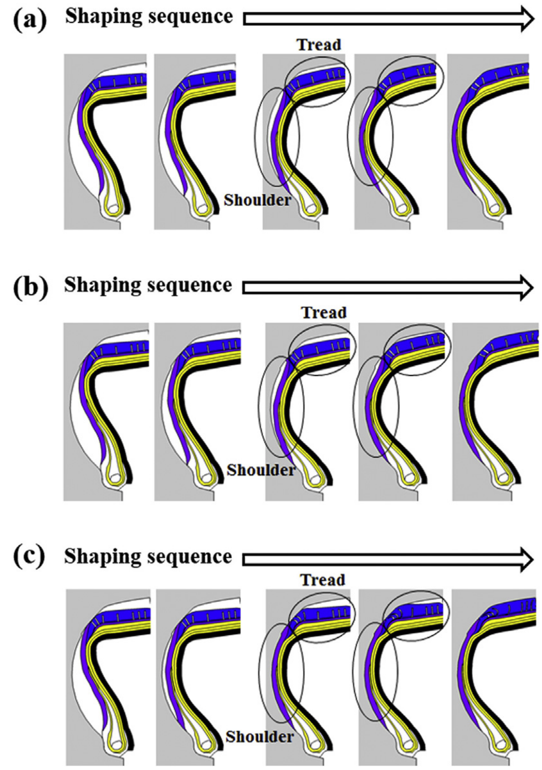

Fig. 17. Shaping sequence of the shoulder area depending on the viscosity of layers. (a) Simulation with unmodified (original) viscosity. (b) Simulation with increased viscosity of the NFC layer. (c) Simulation with increased viscosity of both the NFC and composite layers.

Acknowledgements

This work was supported by the Industrial Fundamental Technology Development Program funded by the Ministry of Trade, Industry and Energy (MOTIE) of Korea. (10051680, Development of high strength and environmental friendly polymer for 3D printing).

References

[1] S.K. Clark (Ed.), Mechanics of Pneumatic Tires, US Dept. of Transportation, National Highway Traffic Safety Administration, Washington, DC, 1981.
[2] L.R. Ray, Nonlinear tire force estimation and road friction identification: simulation and experiments, Automatica 33 (10) (1997) 1819.
[3] X. Xia, J.N. Willis, The effects of tire cornering stiffness on vehicle linear handling performance, SAE Tech. Pap. 950313 (1995).
[4] J.K. Thompson, Plane wave resonance in the tire air cavity as a vehicle interior noise source, Tire Sci. Technol. 23 (1) (1995) 2.
[5] D. Savitskia, D. Schleinina, V. Ivanova, K. Augsburga, E. Jimenezb, R. Heb, C. Sandub, P. Barberc, Improvement of traction performance and off-road mobility for a vehicle with four individual electric motors: driving over icy road, J. Terramech 69 (2017) 33–43.
[6] J.E. Mark, B. Erman, F.R. Erick, The Science and Technology of Rubber, Elsevier Inc, 2005, p. 622.
[7] J. Vavro, J. Vavro, P. Kováčiková, P. Kopas, M. Handrik, Simulation and analysis of defect distribution in passenger car tire under dynamic loading, Appl. Mech. Mater 611 (2014) 544.
[8] M. Ohara, Pneumatic Tire, Tire Mold and Manufacturing Method of Pneumatic Tire, 2011. U.S. 20110247740 A1, Publ.. date October 13.
[9] W.J. Toth, J.P. Chang, C. Zanichelli, Finite element evaluation of the state of cure in a tire, Tire Sci. Technol. 19 (4) (1991) 178.
[10] D. Laurent, M. Sebe, Mold for the Molding and Vulcanizing of a Rubber Tire, 1990. U.S. 4895692 A, Publ.. date January 23.
[11] K.W. Kim, H.S. Jeong, J.-R. Cho, Y.S. Yang, Finite element analysis on residual aligning torque and frictional energy of a tire with detailed tread blocks, Trans. KSAE 12 (4) (2004) 173.

[12] E. Seta, Y. Nakajima, T. Kamegawa, H. Ogawa, Hydroplaning analysis by FEM and FVM: effect of tire rolling and tire pattern on hydroplaning, Tire Sci. Technol. 28 (3) (2000) 140.
[13] E. Seta, T. Kamegawa, Y. Nakajima, Prediction of snow/tire interaction using explicit FEM and FVM, Tire Sci. Technol. 31 (3) (2003) 173.
[14] R. Mundl, M. Fischer, W. Strache, K. Wiese, B. Wies, K.H. Zinken, Virtual pattern optimization based on performance prediction tools, Tire Sci. Technol. 36 (3) (2008) 192.
[15] J. Wu, Y. Wang, B. Su, J. Dong, Z. Cui, B.K. Gond, Prediction of tread pattern block deformation in contact with road, Polym. Test. 58 (2017) 208.
[16] J.K. Lee, D.J. Lee, A study on the friction of tire tread rubber using high-speed friction test machine, J. Korean. Soc. Precis. Eng 30 (6) (2013) 622.
[17] D.-M. Kim, Y.-C. Kwon, D.-Y. Shin, A study on stress analysis of tire tread block, J. Korean. Soc. Aeronautical Space Sci. 25 (5) (1997) 55.
[18] J. Lacombe, Tire model for simulations of vehicle motion on high and low friction road surfaces, Proceedings of the 2000 Winter Simulation Conference (2000) 1025.
[19] S. Weissman, Influence of tire-pavement contact stress distribution on development of distress mechanisms in pavements, J. Transp. Res. Board 1655 (1999) 161.
[20] K.-W. Kim, H.-S. Jeong, Finite element analysis on standing wave phenomenon of a tire considering tread pattern, Trans. KSAE 14 (2) (2006) 76.
[21] B.-S. Kim, Tire tread pitch noise control system by random arrangement of circumference direction straight type groove, J. Korean. Soc. Precis. Eng 11 (6) (1994) 98.
[22] J. Padovan, On standing waves in tires, Tire Sci. Technol. 5 (2) (1977) 83.
[23] J.H. Kim, J.S. Hong, S.H. Choi, H.J. Kim, M.-Y. Lyu, Computer simulation of die extrusion for rubber compound using simplified viscoelastic model, Elast. Compos 46 (1) (2011) 54.
[24] J. Wu, Q. Liu, Y.-S. Wang, Finite element simulation on tire rubber extrusion process, Adv. Mater. Res. 683 (2013) 548.
[25] M.-Y. Lyu, D.-M. Park, H.-J. Kim, J.-R. Yoon, Computer simulation of viscoelastic flow in a capillary die for rubber compounds, Elast. Compos 41 (4) (2006) 223.
[26] D.B. Lee, M.A. Lee, S.H. Choi, M.-Y. Lyu, Computer simulation of rubber flow for mold profile in rubber shaping process, Elast. Compos 49 (3) (2014) 220.
[27] M.-Y. Lyu, J.L. White, Simulation of non-isothermal flow in a modular Buss kneader and comparison with experiment, Int. Polym. Proc. 12 (2) (1997) 104.
[28] M.-Y. Lyu, J.L. White, Non-isothermal non-Newtonian analysis of flow in a modular List/Buss kneader, J. Reinf. Plast. Compos 16 (16) (1997) 1445.